± 5.3 and 18.6 ± 2.2 mg, while their relative weights were 5.7 ± 0.8, 5.0 ± 0.7, 6.1 ± 1.7 and 5.2 ± 0.6 mg/100 g body weight, respectively, and the male low-dose values were significantly lower than the respective male control values. On the other hand, the absolute weights of the thyroid glands of the female control and low-, medium- and high-dose groups were 13.2 ± 3.0, 12.6 ± 3.0, 15.7 ± 3.1 and 13.1 ± 1.9 mg, while their relative weights were 6.9 ± 1.2, 6.4 ± 1.4, 8.2 ± 1.6 and 6.7 ± 0.8 mg/100 g body weight, respectively, and the female medium-dose values were significantly higher than the respective female control values. These slight changes in the thyroid gland weights must lack a biological meaning or relation to the magnetite exposure, because they were not accompanied any other hematological, serological or pathological relatedness, and did not show first-order dose-dependency. No significant or treatment-related changes were observed in any other organ weights.

An apparent macroscopic finding was obtained at necropsy in the high-dose groups of both sexes, with the lungs being slightly enlarged in association with dark brown patches scattered in almost all their lobes (Fig. 3). Additionally, dark brown patches were also observed in the parathymic lymph nodes of male and female rats in the high-dose groups. No significant or treatment-related changes were macroscopically observed in any other organs or tissues.

The histopathological changes detected in the lungs are summarized in Table 2. In the lungs of all rats in all magnetite-treated groups, infiltration of brownishly pigmented macrophages phagocytosing magnetite was observed in the alveolar spaces, walls and interstitium (Figs. 4B, 4C, 4D). Such infiltration was not present in the control groups, and among the magnetite-treated groups, the severity of this change generally increased with the increasing doses of magnetite. Chronic inflammation was observed in 4/17 (23.5%) and 20/20 (100%) of the medium- and high-dose males and 3/17 (17.6%; statistically insignificant), 3/17 (17.6%; statistically insignificant) and 12/12 (100%) of the low-, medium- and high-dose females, respectively. The chronic inflammation was evidenced by an infiltration of inflammatory cells, such as lymphocytes or neutrophils, and fibrosis. This chronic inflammation was frequently associated with macrophages (either phagocytosing magnetite or not) diffusely scattered within the alveolar lumens, and thence multiple focal clusters of alveoli filled with inflammatory cells (mostly macrophages but occasionally mixed with small to moderate numbers of neutrophils) were commonly observed with debris (Figs. 5A, 5B). Hypertrophy and hyperplasia of alveolar epithelial cells (presumably type II pneumocytes) were usually seen in alveoli containing such inflammatory exudates, which were not considered separate/independent lesions but regenerative responses secondary to the inflammation. Alveolar bronchiolization, identified by the lining of normal or thickened alveolar walls with cells resembling the bronchiolar epithelium (Figs. 5C, 5D), was observed in 2/17 (11.8%; statistically insignificant) and 15/20 (75.0%) of the medium- and high-dose males and 3/17 (17.6%; statistically insignificant) and 12/12 (100%) of the medium- and high-dose females, respectively. The bronchiolized epithelium consisted of a single layer of ciliated and nonciliated columnar cells, and extended from the terminal bronchiole onto the septa of the adjacent alveoli (Figs. 5C, 5D). As an additional inflammatory change, granuloma was observed in 7/20 (35%) and 6/12 (50%) of the high-dose males and females, respectively. On the other hand, alveolar

Table 2. Histological Findings of the Lungs and Parathymic Lymph Nodes

Item	Dose of magnetite (mg/kg body weight)			
	0 (control)	0.2	1.0	5.0
Male				
Effective number of rats	20	17	17	20
Lung				
Infiltration of macrophages phagocytosing magnetite	0[a]	17*	17*	20*
Chronic inflammation	0	0	4*	20*
Alveolar bronchiolization	0	0	2	15*
Granuloma	0	0	0	7*
Bronchoalveolar hyperplasia	3	0	0	2
Parathymic lymph nodes				
Infiltration of macrophages phagocytosing magnetite	0	17*	17*	20*
Female				
Effective number of rats	14	17	17	12
Lung				
Infiltration of macrophages phagocytosing magnetite	0	17*	17*	12*
Chronic inflammation	0	3	3	12*
Alveolar bronchiolization	1	0	3	12*
Granuloma	0	0	0	6*
Bronchoalveolar hyperplasia	0	0	0	2
Parathymic lymph nodes				
Infiltration of macrophages phagocytosing magnetite	0	17*	17*	12*

[a] Number of rats with a lesion. * Significantly different from the corresponding control values ($P<0.05$, Fisher's exact test). No apparent histological changes were observed in the other organs when compared with the control rats.

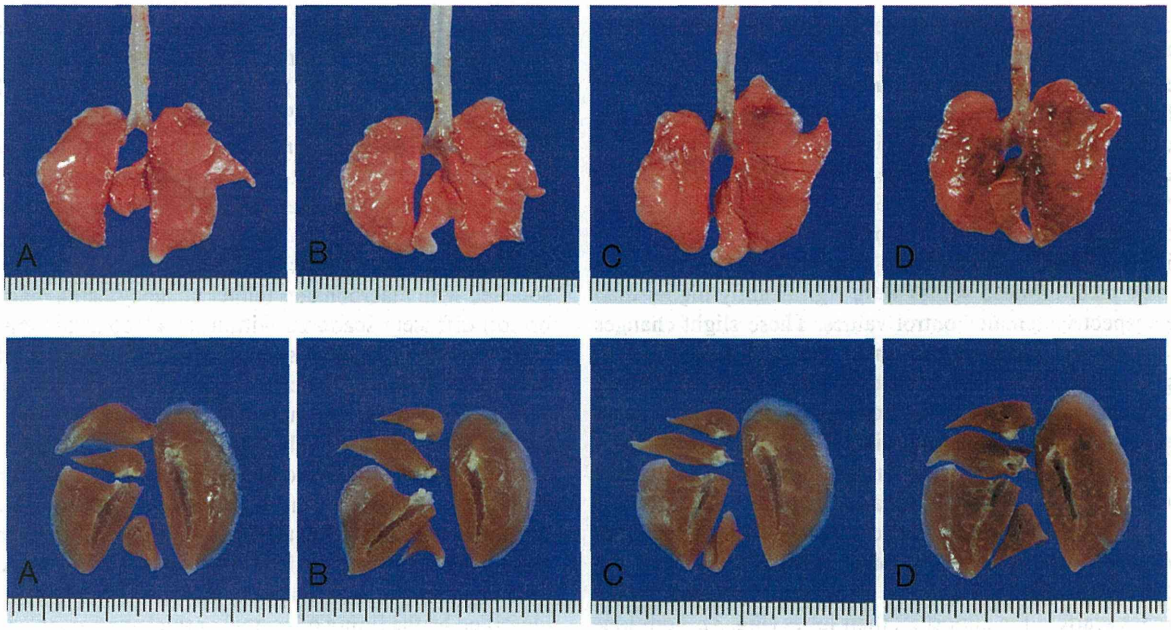

Fig. 3. Representative gross views (upper row) and cross-sections of the formalin-fixed tissues (lower row) of the lungs. The doses of magnetite were 0 (control) (A), 0.2 (B), 1.0 (C) and 5.0 (D) mg/kg body weight per administration.

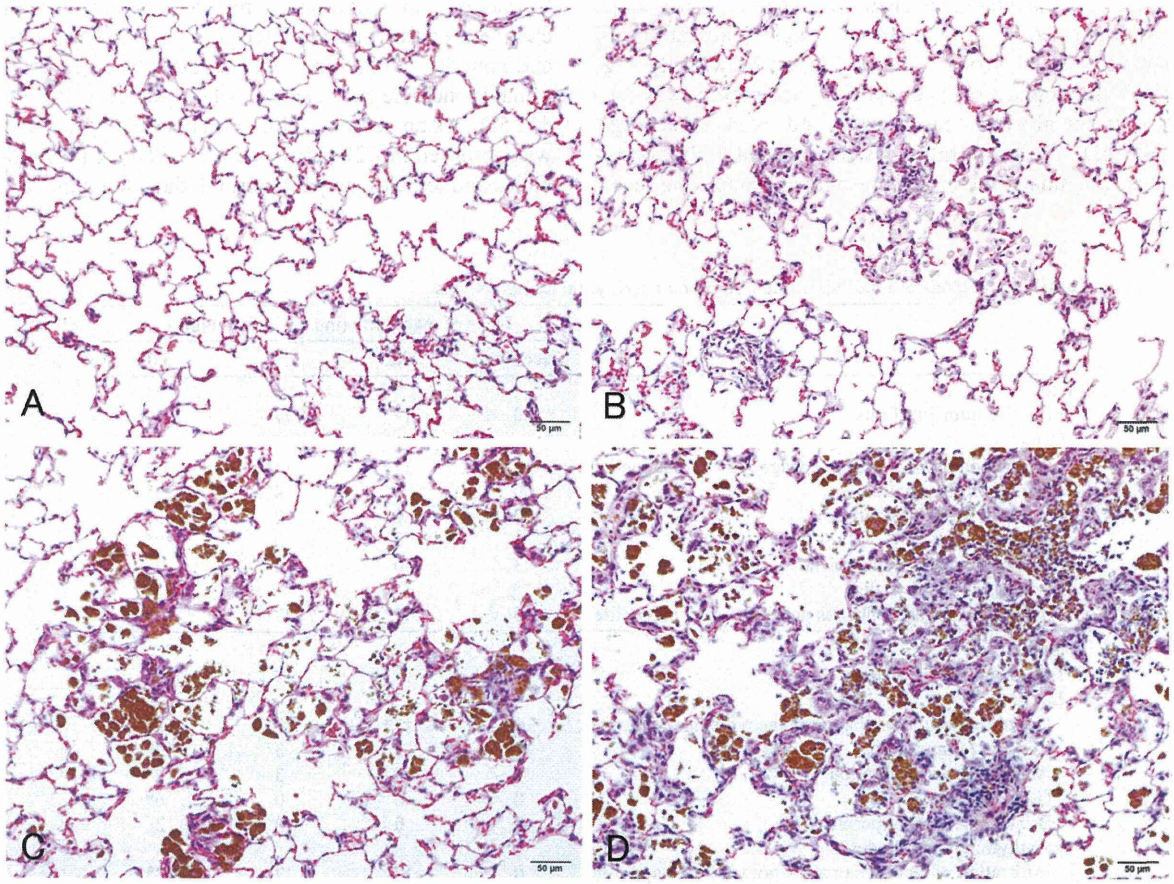

Fig. 4. Representative microscopic views of the lungs of the control (A) and low- (B), medium- (C) and high-dose (D) groups (hematoxylin and eosin).

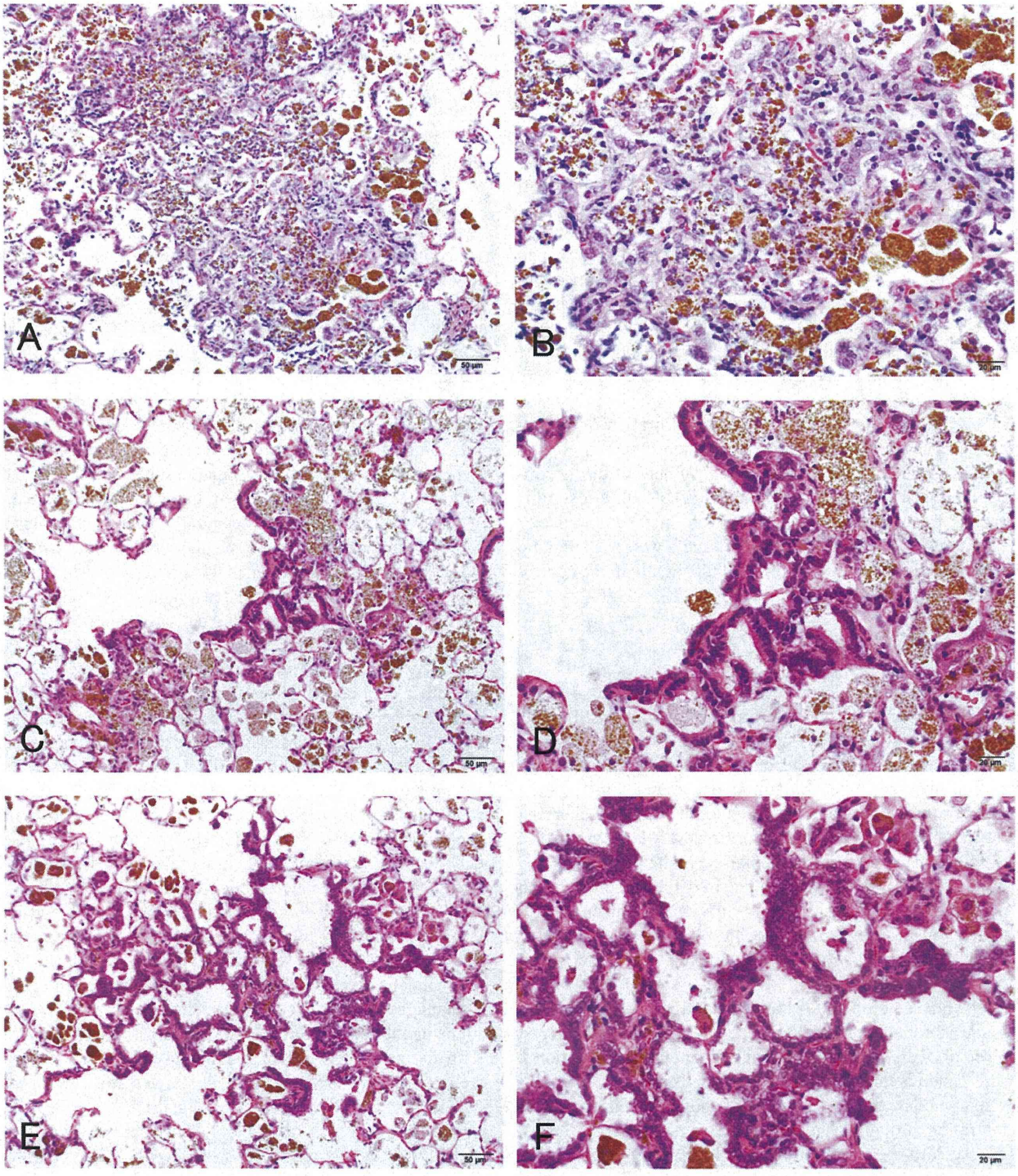

Fig. 5. Representative lesions observed in the lungs of the high-dose group (hematoxylin and eosin): infiltration of macrophage phagocytosing magnetite (A–F), chronic inflammation (A, B), alveolar bronchiolization (C, D) and alveolar hyperplasia (E, F). The right row shows higher magnification versions of the left row images. The bronchiolization was identified as a non-proliferative lesion, in which the lining of alveolar walls was replaced by cells resembling the bronchiolar epithelium. The alveolar hyperplasia was identified as a lesion consisting of proliferative alveolar epithelial cells.

hyperplasia was observed in 2/20 (10%; statistically insignificant) and 2/12 (16.7%; statistically insignificant) of the high-dose males and females, respectively, as well as 3/20 (15%; statistically insignificant) of the control males. While the alveolar hyperplasias did not compress the surrounding parenchyma, those observed in the control males were focal, and those found in the high-dose males and females tended to extend to the surroundings with poor demarcation and were accompanied by inflammation (Figs. 5E, 5F). The hyperplastic alveolar epithelial cells (presumably type II pneumocytes) were cuboidal and round-to-oval shaped hyperchromatic nuclei (Figs. 5E, 5F), and cytoplasmic overexpression of β-catenin protein was immunohistochemically found (Figs. 6C, 6D), whereas the protein was mainly localized at the membranes of the cell-cell borders in the background lung tissue irrespective of magnetite exposure (Figs. 6A, 6B).

In the parathymic lymph nodes, infiltration of macrophages phagocytosing magnetite was observed in all rats in all magnetite-treated groups (Fig. 7) but not in the control animals, as shown in the lungs (Table 2). No significant or treatment-related changes were histopathologically observed in any other organs or tissues, whereas sporadic spontaneous lesions were observed identically in the control and treated rats.

Discussion

The present study clearly revealed that a total of 13 quadweekly intermittent intratracheal spray instillations of magnetite (Fe_3O_4) nanoparticles for 52 weeks at doses of 0, 0.2, 1.0 and 5.0 mg/kg body weight per administration caused dose-dependent inflammatory changes in the lung and parathymic lymph node of male and female Fischer 344 rats but not in the other organs or tissues. A large amount of the administered magnetite remained in the lung, and some of the magnetite was distributed into the regional lymph nodes. Histopathologically, infiltration of macrophages phagocytosing magnetite and of chronic inflammatory cells, alveolar bronchiolization and granuloma were observed in the lungs of treated rats.

Alveolar bronchiolization is identified as cells resembling a bronchiolar epithelia line on normal or thickened alveolar walls, which often manifest an acinar formation[19]. This lesion is thought to arise from the "colonization" of alveolar walls within the bronchiolar epithelium either via cell migration through alveolar pores or from the transformation of alveolar type II cells into bronchiolar-type epithelium[19]. This is seen in various types of experimental lung injury caused by viral infection[20] or exposure to ozone[21], chromate[19] and paraquat[22]; it is also seen in human lung cancer cases[23]. Jensen-Taubman *et al.* examined the incidence and association of alveolar bronchiolization with non-small cell lung cancer (NSCLC) in lung resection specimens from 2 patient groups, those with NSCLC and those diagnosed with a variety of non-neoplastic lung conditions[23]. They observed that alveolar bronchiolization occurs in up to 8% (1/12) of non-lung-cancer cases and 12% (5/42) of NSCLC cases. They described that alveolar bronchiolization does not necessarily occur only in adenocarcinoma cases, suggesting that this form of alveolar metaplasia may somehow be associated with a spectrum of NSCLC histologic subtypes. The precise roles of alveolar bronchiolization in lung carcinogenesis are not known at this moment, and thus this lesion is currently considered to be an inflammatory response.

In line with the content of the last paragraph, alveolar hyperplasia was observed in male and female rats exposed to the high dose of magnetite, whereas the incidences were low and not significantly different from those in the respective control groups. A similar lesion was observed also in control males (but not females), but the histopahological appearances of the lesions seen in the treated groups were somewhat qualitatively different from those seen in male control animals. A "primary" alveolar hyperplasia is considered a precursor lesion of lung cancers and must be differentiated from regenerative hyperplasia. A preneoplastic hyperplasia is usually not associated with inflammation or necrosis, and the parenchymal architecture is maintained[24]. While alveolar hyperplasias seen in the high-dose groups of the present study were accompanied by chronic inflammation, a number of molecular pathways activated in chronic inflammation have been indicated to contribute to lung carcinogenesis[25]. Alveolar epithelial cells contribute to the initiation and modulation of inflammatory responses, which in turn may result in the release of cytokines, growth factors and other peptide mediators that may predispose epithelial cells themselves to a proliferative response[26,27]. Foreign particles, infectious agents and chemicals can induce an inflammatory response in the lung leading to oxidative stress. Also with regard to magnetite, exposure to it has been shown to induce oxidative stress and deplete antioxidant levels in the lung epithelial cells, stimulating the apoptotic pathway for cell death[14]. Furthermore, magnetite particles have been revealed to induce concentration-dependent DNA damage and enhance reactive oxygen species production[6] and micronuclei induction[28]. It may be particularly of importance that β-catenin protein was overexpressed in the epithelial cells of the presently observed alveolar hyperplasia in the high magnetite dose groups, while the protein was localized in the membranes of the cell-cell borders of the background lung tissue irrespective of magnetite exposure. It is very well known that β-catenin protein is a versatile component of homotypic cell adhesion and signaling, the subcellular localization and cytoplasmic levels of which are tightly regulated by adenomatous polyposis coli (APC) protein. Mutations occurring in the *β-catenin* and/or *APC* genes result in aberrant overexpression of β-catenin protein first in the cytoplasms and then its translocation into the nuclei, causing nuclear accumulation of the protein and in turn improper gene activation[29]. Typically, for instance, the accumulated β-catenin protein in the nuclei interacts with the Tcf family members, resulting in the acquisition of growth advantage of target genes[30]. Likewise, immunohistochemical studies of *N*-nitrosobis (2-hydroxypropyl) amine-induced rat lung

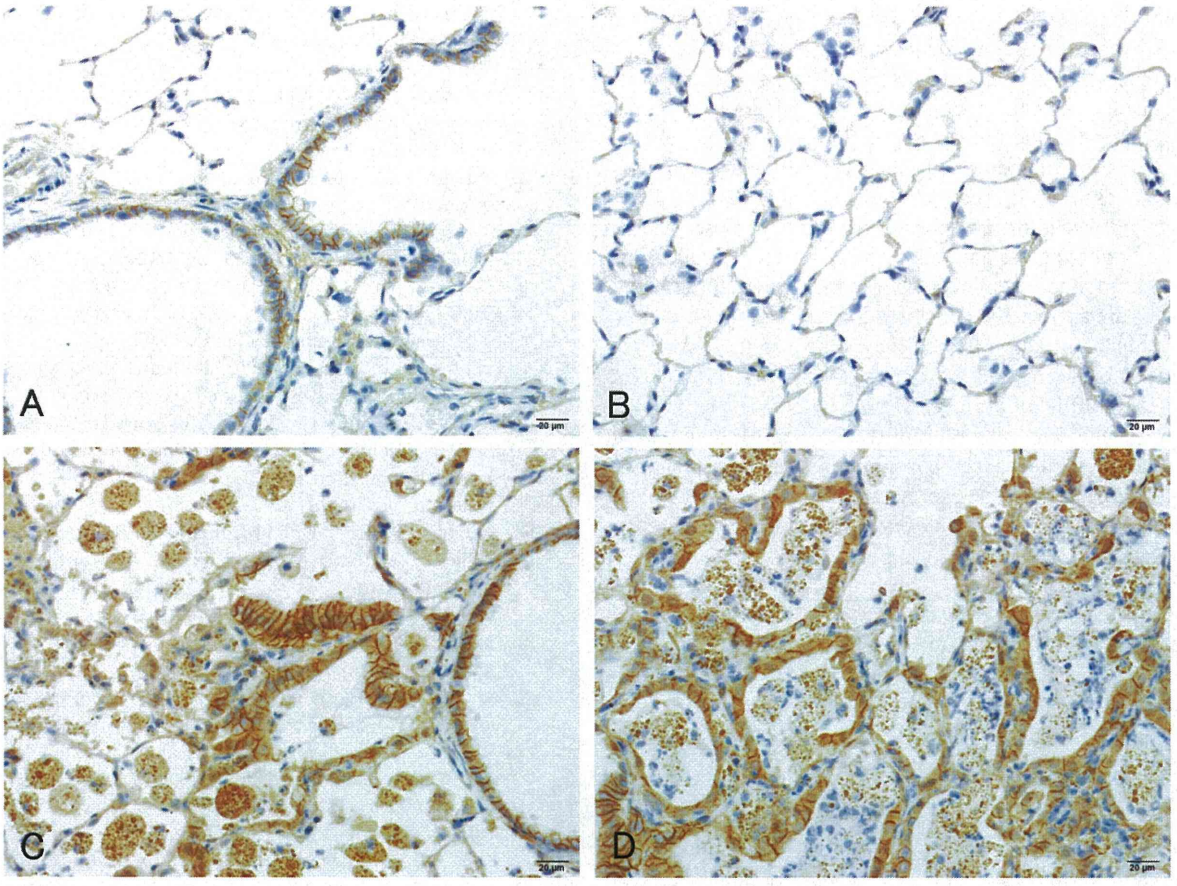

Fig. 6. Representative results of β-catenin immunohistochemistry of the lungs of the control (A, B) and high-dose (C, D) groups. The β-catenin protein was localized at the membranes of the cell-cell borders in the background lung tissue (A–D), whereas cytoplasmic overexpression of the protein was found in the hyperplastic alveolar epithelial cells (C, D).

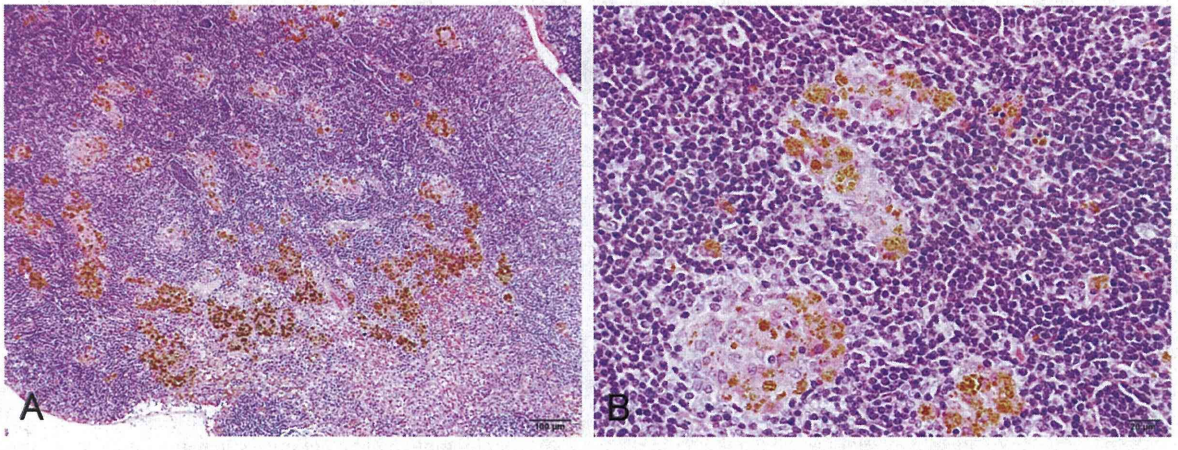

Fig. 7. Representative microscopic views of the parathymic lymph node of the high-dose group (hematoxylin and eosin). Infiltration of macrophages phagocytosing magnetite and deposits of magnetite particles are evident.

tumors[30] and of azoxymethane-induced rat colon tumors[31,32] have revealed frequent translocation of the β-catenin protein from the cell membranes to the cytoplasms and then the nuclei in adenomas and adenocarcinomas, but not in hyperplasia, suggesting the mechanistic involvement of the nuclear accumulation of the protein in those chemical carcinogenesis processes. In this context, the presently observed alveolar hyperplasias in rats exposed to the high dose of magnetite might possess a potent preneoplastic potential. When considering the potential risk for humans, therefore, further studies are apparently warranted to elucidate whether or not intratracheally administered magnetite has the potency to cause lung carcinogenesis, and such studies are being conducted in our laboratories.

In conclusion, the present results clearly show that instilled magnetite causes chronic inflammatory responses in the lung. These long-term pulmonary responses occur in a dose-dependent manner without apparent differences among sexes.

Acknowledgments: The authors would like to express their gratitude to Dr. Yukari Totsuka (Cancer Prevention Basic Research Project, National Cancer Center Research Institute, Tokyo, Japan) for arrangement of the supply of magnetite and helpful suggestions. We also thank Mr. Toshiyuki Hakata and the staff of Toda Kogyo Co., Inc. (Hiroshima, Japan), for their generous supply of magnetite and its technical information. This work was supported in part by a Health and Labour Sciences Research Grant (awarded to Dai Nakae) from the Ministry of Health, Labour and Welfare of Japan.

References

1. Hood E. Nanotechnology: looking as we leap. Environ Health Perspect. **112**: A740–A749. 2004. [Medline] [CrossRef]
2. Lin BL, Shen XD, and Cui S. Application of nanosized Fe_3O_4 in anticancer drug carriers with target-orientation and sustained-release properties. Biomed Mater. **2**: 132–134. 2007. [Medline] [CrossRef]
3. Kikumori T, Kobayashi T, Sawaki M, and Imai T. Anti-cancer effect of hyperthermia on breast cancer by magnetite nanoparticle-loaded anti-HER2 immunoliposomes. Breast Cancer Res Treat. **113**: 435–441. 2009. [Medline] [CrossRef]
4. Hilger I, and Kaiser WA. Iron oxide-based nanostructures for MRI and magnetic hyperthermia. Nanomedicine (Lond). **7**: 1443–1459. 2012. [Medline] [CrossRef]
5. Hong SC, Lee JH, Lee J, Kim HY, Park JY, Cho J, Lee J, and Han DW. Subtle cytotoxicity and genotoxicity differences in superparamagnetic iron oxide nanoparticles coated with various functional groups. Int J Nanomedicine. **6**: 3219–3231. 2011. [Medline]
6. Könczöl M, Ebeling S, Goldenberg E, Treude F, Gminski R, Gieré R, Grobéty B, Rothen-Rutishauser B, Merfort I, and Mersch-Sundermann V. Cytotoxicity and genotoxicity of size-fractionated iron oxide (magnetite) in A549 human lung epithelial cells: Role of ROS, JNK, and NF-κB. Chem Res Toxicol. **24**: 1460–1475. 2011. [Medline] [CrossRef]
7. Slesinski RS, and Turnbull D. Chronic inhalation exposure of rats for up to 104 weeks to a non-carbon-based magnetite photocopying toner. Int J Toxicol. **27**: 427–439. 2008. [Medline] [CrossRef]
8. Pauluhn J. Subchronic inhalation toxicity of iron oxide (magnetite, Fe_3O_4) in rats: pulmonary toxicity is determined by the particle kinetics typical of poorly soluble particles. J Appl Toxicol. **32**: 488–504. 2012. [Medline] [CrossRef]
9. Chen BA, Jin N, Wang J, Ding J, Gao C, Cheng J, Xia G, Gao F, Zhou Y, Chen Y, Zhou G, Li X, Zhang Y, Tang M, and Wang X. The effect of magnetic nanoparticles of Fe_3O_4 on immune function in normal ICR mice. Int J Nanomedicine. **5**: 593–599. 2010. [Medline] [CrossRef]
10. Pott F, Ziem U, Reiffer FJ, Huth F, Ernst H, and Mohr U. Carcinogenicity studies on fibres, metal compounds, and some other dusts in rats. Exp Pathol. **32**: 129–152. 1987. [Medline] [CrossRef]
11. Steinhoff D, Mohr U, and Hahnemann S. Carcinogenesis studies with iron oxides. Exp Pathol. **43**: 189–194. 1991. [Medline] [CrossRef]
12. Tada Y, Yano N, Takahashi H, Yuzawa K, Ando H, Kubo Y, Nagasawa A, Ogata A, and Nakae D. Acute phase pulmonary responses to a single intratracheal spray instillation of magnetite (Fe_3O_4) nanoparticles in Fischer 344 rats. J Toxicol Pathol. **25**: 233–239. 2012. [Medline] [CrossRef]
13. Singh N, Jenkins GJ, Asadi R, and Doak SH. Potential toxicity of superparamagnetic iron oxide nanoparticles (SPION). Nano Rev. **1**: 5358–5373. 2010. [Medline]
14. Ramesh V, Ravichandran P, Copeland CL, Gopikrishnan R, Biradar S, Goornavar V, Ramesh GT, and Hall JC. Magnetite induces oxidative stress and apoptosis in lung epithelial cells. Mol Cell Biochem. **363**: 225–234. 2012. [Medline] [CrossRef]
15. Organisation for Economic Co-operation and Development (OECD). List of Manufactured Nanomaterials and List of Endpoints for Phase One of the Sponsorship Programme for the Testing of Manufactured Nanomaterials: Revision. Paris. 1–16. 2010.
16. Japanese Association for Laboratory Animal Science (JALAS) Guidelines for animal experimentation. Exp Anim. **36**: 285–288. 1987.
17. Driscoll KE, Costa DL, Hatch G, Henderson R, Oberdorster G, Salem H, and Schlesinger RB. Intratracheal instillation as an exposure technique for the evaluation of respiratory tract toxicity: uses and limitations. Toxicol Sci. **55**: 24–35. 2000. [Medline] [CrossRef]
18. Gad SC, and Weil CS. Statistics for toxicologist. In: Principles and Methods of Toxicology, 3rd ed. AW Hayes (ed). Raven Press, New York. 221–274. 1994.
19. Nettesheim P, and Szakal AK. Morphogenesis of alveolar bronchiolization. Lab Invest. **26**: 210–219. 1972. [Medline]
20. Baskerville A, Thomas G, Wood M, and Harris WJ. Histology and ultrastructure of metaplasia of alveolar epithelium following infection of mice and hamsters with influenza virus. Br J Exp Pathol. **55**: 130–137. 1974. [Medline]
21. Pinkerton KE, Dodge DE, Cederdahl-Demmler J, Wong VJ, Peake J, Haselton CJ, Mellick PW, Singh G, and Plopper CG. Differentiated bronchiolar epithelium in alveolar ducts of rats exposed to ozone for 20 months. Am J Pathol. **142**: 947–956. 1993. [Medline]

22. Fukuda Y, Takemura T, and Ferrans VJ. Evolution of metaplastic squamous cells of alveolar walls in pulmonary fibrosis produced by paraquat. Virchows Arch B. **58**: 27–43. 1989. [Medline] [CrossRef]
23. Jensen-Taubman SM, Steinberg SM, and Linnoila RI. Bronchiolization of the alveoli in lung cancer: pathology, patterns of differentiation and oncogene expression. Int J Cancer. **75**: 489–496. 1998. [Medline] [CrossRef]
24. Dixon D, Herbert RA, Sills RC, and Boorman GA. Lungs, pleura, and mediastinum. In: Pathology of the Mouse: Reference and Atlas. RR Maronpot, GA Boorman, and BW Gaul (eds). Cache River, Vienna. 293-332. 1999.
25. Ballaz S, and Mulshine JL. The potential contributions of chronic inflammation to lung carcinogenesis. Clin Lung Cancer. **5**: 46–62. 2003. [Medline] [CrossRef]
26. Simon RH, and Paine R. Participation of pulmonary alveolar epithelial cells in lung inflammation. J Lab Clin Med. **126**: 108–118. 1995. [Medline]
27. Shacter E, and Weitzman SA. Chronic inflammation and cancer. Oncology. **16**: 217–226, 229–232. 2002. [Medline]
28. Kawanishi M, Ogo S, Ikemoto M, Totsuka Y, Ishino K, Wakabayahsi K, and Yagi T. Genotoxicity and reactive oxygen species production induced by magnetite nanoparticles in mammalian cells. J Toxicol Sci. 2013; in press. [Medline] [CrossRef]
29. Ilyas M, and Tomlinson IPM. The interactions of APC, E-cadherin and β-catenin in tumor development and progression. J Pathol. **182**: 128–137. 1997. [Medline] [CrossRef]
30. Tsujiuchi T, Tsutsumi M, Sasaki Y, Murata N, and Konishi Y. Mutations of adenomatous polyposis coli and beta-catenin genes during progression of lung tumors induced by *N*-nitrosobis(2-hydroxypropyl)amine in rats. Cancer Res. **60**: 6611–6616. 2000. [Medline]
31. Takahashi M, Fukuda K, Sugimura T, and Wakabayashi K. Beta-catenin is frequently mutated and demonstrates altered cellular location in azoxymethane-induced rat colon tumors. Cancer Res. **58**: 42–46. 1998. [Medline]
32. Takahashi M, Mutoh M, Kawamori T, Sugimura T, and Wakabayashi K. Altered expression of beta-catenin, inducible nitric oxide synthase and cyclooxygenase-2 in azoxymethane-induced rat colon carcinogenesis. Carcinogenesis. **21**: 1319–1327. 2000. [Medline] [CrossRef]

Arch Toxicol
DOI 10.1007/s00204-013-1096-3

IN VITRO SYSTEMS

Effects of *N*-acetyl-L-cysteine on target sites of hydroxylated fullerene-induced cytotoxicity in isolated rat hepatocytes

Yoshio Nakagawa · Toshinari Suzuki · Kazuo Nakajima · Akiko Inomata · Akio Ogata · Dai Nakae

Received: 14 May 2013 / Accepted: 11 July 2013

Abstract The effects of *N*-acetyl-L-cysteine (NAC) on cytotoxicity caused by a hydroxylated fullerene [$C_{60}(OH)_{24}$], which is known a nanomaterial and/or a water-soluble fullerene derivative, were studied in freshly isolated rat hepatocytes. The exposure of hepatocytes to $C_{60}(OH)_{24}$ at a concentration of 0.1 mM caused time (0–3 h)-dependent cell death accompanied by the formation of cell blebs, loss of cellular ATP, and reduced glutathione (GSH) and protein thiol levels, as well as the accumulation of glutathione disulfide and malondialdehyde (MDA), indicating lipid peroxidation. Despite this, $C_{60}(OH)_{24}$-induced cytotoxicity was effectively prevented by NAC pretreatment ranging in concentrations from 1 to 5 mM. Further, the loss of mitochondrial membrane potential (MMP) and generation of oxygen radical species in hepatocytes incubated with $C_{60}(OH)_{24}$ were inhibited by pretreatment with NAC, which caused increases in cellular and/or mitochondrial levels of GSH, accompanied by increased levels of cysteine via enzymatic deacetylation of NAC. On the other hand, severe depletion of cellular GSH levels caused by diethyl maleate at a concentration of 1.25 mM led to the enhancement of $C_{60}(OH)_{24}$-induced cell death accompanied by a rapid loss of ATP. Taken collectively, these results indicate that pretreatment with NAC ameliorates (a) mitochondrial dysfunction linked to the depletion of ATP, MMP, and mitochondrial GSH level and (b) induction of oxidative stress assessed by reactive oxygen species generation, losses of intracellular GSH and protein thiol levels, and MDA formation caused by $C_{60}(OH)_{24}$, suggesting that the onset of toxic effects is at least partially attributable to a thiol redox-state imbalance as well as mitochondrial dysfunction related to oxidative phosphorylation.

Keywords Hydroxylated fullerene · Fullerenol · Mitochondrial dysfunction · Oxidative stress · *N*-acetyl-L-cysteine · Cytotoxicity · Rat hepatocytes

Abbreviations

DEM	Diethyl maleate
DCHF-DA	2′,7′-Dichlorodihydrofluorescein diacetate
DNP-NAC	2,4-Dinitrophenyl *S*-conjugate of *N*-acetyl-L-cysteine
DMSO	Dimethyl sulfoxide
GSH	Glutathione
GSSG	Glutathione disulfide
HEPES	*N*-(2-hydroxyethyl)-piperazine-*N*-(2-ethanesulfonic acid)
MDA	Malondialdehyde
MPT	Mitochondrial permeability transition
NAC	*N*-acetyl-L-cysteine
ROS	Reactive oxygen species
MMP	Mitochondrial membrane potential

Y. Nakagawa (✉) · A. Inomata · A. Ogata · D. Nakae
Division of Toxicology, Tokyo Metropolitan Institute of Public Health, 3-24-1, Hyakunin-cho, Shinjuku-ku, Tokyo 169-0073, Japan
e-mail: Yoshio_1_Nakagawa@member.metro.tokyo.jp

T. Suzuki
Division of Environmental Health, Tokyo Metropolitan Institute of Public Health, 3-24-1, Hyakunin-cho, Shinjuku-ku, Tokyo 169-0073, Japan

K. Nakajima
Division of Food Additives, Tokyo Metropolitan Institute of Public Health, 3-24-1, Hyakunin-cho, Shinjuku-ku, Tokyo 169-0073, Japan

Published online: 23 July 2013

Introduction

Fullerenes, C_{60} and/or larger, are nanospheres as well as nanomaterials derived from carbon atoms and have been the focus of increasing interest for possible applications in multipronged industrial fields such as electronic engineering, pharmaceuticals, medical devices, cosmetics, and other boundary region industries since their discovery in 1985 (Kroto et al. 1985). While fullerene derivatives synthesized by the addition of reactive functional groups, such as hydroxyl-, carboxyl-, amino-, and alkyl-groups and other side-chain/cyclic moieties, to the C_{60} structure are widely produced in amounts of several tons per year (Borm et al. 2006), actual commercialization is still mostly under development. This trend is expected to result in the ever-increasing presence of nanomaterials in the human environment, although relatively little is known about the potential biological risks of nanomaterials, including fullerenes and their derivatives. Therefore, the relationship between these nanomaterials and their target sites in the body and/or tissues and cells has recently become an important theme of biological and/or toxicologic research.

Although fullerenes are generally hydrophobic molecules and are not water-soluble, chemical modification of the fullerene C_{60} molecule through the participation of hydrophilic addends such as hydroxyl groups leads to various polyhydroxylated fullerenes, also termed either fullerenols or fullerols, such as $C_{60}(OH)_n$, some of which show improved solubility in biological media. The enhancement of hydrophilicity was correlated with an increase in the number of hydroxyl groups in fullerenes, which induce their biological activities. Some fullerenols are potential candidates for pharmacological applications, including scavengers of oxygen radical species (Murugan et al. 2002; Tsai et al. 1997), protective agents against chemical-induced organ (Injac et al. 2008, 2009) and/or cell damages (Bogdanović et al. 2004), and neuroprotective and anticancer agents (Chen et al. 2005; Jin et al. 2000). Sayes et al. (2004) reported that in cell lines derived from human dermal fibroblasts, the cytotoxicity of water-soluble fullerenols [$C_{60}(OH)_n$] may be associated with specific functions of surface derivatization on C_{60}. On the other hand, fullerenols such as $C_{60}(OH)_{7 \pm 2}$ and $C_{60}(OH)_{24}$ caused cytotoxicity in RAW 264.7 cells (Chen et al. 2004) and in vascular endothelial cells (Yamawaki and Iwai 2006), respectively. Furthermore, fullerenols are thought to have cytotoxic/phototoxic (Isakovic et al. 2006; Roberts et al. 2008), genotoxic, and mutagenic effects in CHO, Hela, and HEK293 cell lines, respectively (Mrdanović et al. 2009; Niwa and Iwai 2007). Thus, the results from in vitro studies suggest that fullerenols exert cytotoxic as well as protective effects on various cell lines.

The liver is a major organ for the metabolism and detoxification of drugs and xenobiotics absorbed from the alimentary tract, and it may be highly susceptible to injury by these compounds at any time. When nanomaterials are inhaled through respiration, absorbed through the skin, or administered by intravenous injection, they enter the blood stream and are translocated to the liver (Sadauskas et al. 2007). Because blood containing these compounds passes through the liver before being distributed throughout the body, the liver is a potential target organ of nanomaterials. It was shown that some nanoparticles present in rat liver after intravenous administration induce oxidative stress locally after nanoparticle phagocytosis (Hoet et al. 2004). The freshly isolated rat hepatocyte system, which retains intact membranes and has high levels of various drug-metabolizing enzymes and their cofactors and multiple defense systems against intracellular oxidative stress produced by various chemicals as well as intact liver cells in the body, is useful for the study of the pharmacokinetics, intracellular target sites, morphologic/physiologic degeneration, and temporal sequences leading to cell injury induced by xenobiotics.

Although in vivo and in vitro studies confirmed that fullerenes and their derivatives could cross the external cellular membrane and accumulate in cells and/or tissues (Foley et al. 2002; Yamawaki and Iwai 2006), little is known of their cytotoxic effects and mechanisms of action on rat hepatocytes. Our previous study indicated that fullerenols such as $C_{60}(OH)_{24}$ and $C_{60}(OH)_{12}$ elicit cytotoxicity through mitochondrial failure related to the induction of the membrane permeability transition (MPT), mitochondrial depolarization, and inhibition of ATP synthesis, accompanied by rapid oxidation of cellular glutathione (GSH) and protein thiols (Nakagawa et al. 2011). It is well known that reduced GSH, a major cellular antioxidant and/or nucleophilic agent, is affected immediately by various forms of oxidative stress and xenobiotic detoxification in liver cells. In connection with this, *N*-acetyl-L-cysteine (NAC) is used as an effective acetylated precursor for reduced GSH in hepatocytes, and its application in different diseases including cancer, cardiovascular disorders, and chemical and metal toxicity has been reviewed previously (Zafarullah et al. 2003). In the present study, we investigated the protective effects of NAC against hydroxylated fullerene $C_{60}(OH)_{24}$-induced cytotoxicity in isolated rat hepatocytes. The mechanism of fullerene toxicity is also discussed.

Materials and methods

Materials

The chemical compounds used were obtained from the following companies: hydroxylated fullerene $C_{60}(OH)_{24}$ (fullerenol, purity of >99.5 %) from Materials Technologies

Research Ltd. (Cleveland, OH, USA), collagenase, NAC, L-cysteine and 1-fluoro-2,4-dinitrobenzene from Wako Pure Chemical Industries Ltd. (Osaka, Japan), glutathione (GSH), glutathione disulfide (GSSG), *N*-(2-hydroxyethyl)-piperazine-*N*-(2-ethanesulfonic acid) (HEPES), bovine serum albumin, diethyl maleate (DEM), 2′,7′-Dichlorodihydrofluorescein diacetate (DCHF-DA), and rhodamine 123 from Sigma Chemical Co. (St. Louis, MO, USA). All other chemicals were of the highest purity commercially available. Molecular formula of the fullerenol used in this study was assumed to be that reported by the manufacturer.

Isolation and cell culture incubation of hepatocytes

Male F344/Jcl (200–250 g) rats were obtained from CLEA Japan Inc. (Tokyo, Japan) and were housed in wire-bottom cages. The rats were allowed food (CE-2, CLEA Japan Inc., Tokyo) and water ad libitum. All animal husbandry and experimental procedures were approved under the Tokyo Metropolitan Institute of Public Health guidelines for the care and use of laboratory animals. After the rats were anesthetized with diethyl ether by inhalation, hepatocytes (1×10^6 cells/ml) were isolated by in situ two-step collagenase perfusion of the liver and suspended in Krebs–Henseleit buffer, pH 7.4, containing 12.5 mM HEPES and 0.1 % albumin, as described previously (Moldéus et al. 1978). All incubations were performed in rotating, round-bottomed flasks at 37 °C, under a constant flow of humidified carbogen (95 % O_2/5 % CO_2). The fullerenol $C_{60}(OH)_{24}$ was dissolved in dimethyl sulfoxide (DMSO) and sonicated for 30 min before the addition to hepatocyte suspensions. Reactions were initiated by addition of $C_{60}(OH)_{24}$ dissolved in DMSO (final concentration <0.5 %). In some experiments, prior to the addition of the fullerenol, the isolated hepatocytes were preincubated with NAC (final concentrations 1–5 mM) dissolved in Krebs–Henseleit buffer for 20 min or diethyl maleate (DEM, final concentration 1.25 mM) dissolved in DMSO for 15 min, respectively. The concentrations of NAC and DEM used here were obtained from previous studies (Nakagawa et al. 1993; Tirmenstein et al. 2000). Corresponding control groups received an equivalent volume of DMSO or Krebs–Henseleit buffer. Aliquots of incubation mixture were taken at intervals to monitor cell death and the concentrations of intracellular adenine nucleotides, GSH, GSSG, cysteine, reduced protein thiols, NAC, malondialdehyde (MDA), and reactive oxygen species (ROS).

Biochemical and morphological assays

Adenine nucleotides (ATP, ADP, and AMP) in hepatocytes were determined using a modified HPLC system, as described by Jones (1981). GSH, GSSG, and cysteine levels were determined by HPLC essentially as described by Reed et al. (1980). Reduced protein thiol concentrations were determined by using Ellman's reagent [5,5′-dithiobis-(2-nitrobenzoic acid)], as described previously (Albano et al. 1985). Protein was determined by the method of Lowry et al. (1951), using bovine serum albumin as the standard. MDA was measured as thiobarbituric acid-reactive products, as described previously (Sandy et al. 1986), and the amount of reactive product formed was calculated by using an extinction coefficient of 156 mM/cm. To assess hepatocyte viability, an equal volume of trypan blue solution (final concentration 0.08 %) was added into an aliquot of hepatocyte suspensions and the mixture was loaded into a hemacytometer. Cell viability was assayed by counting the number of cells excluding trypan blue in a Burker's chamber placed under a light microscope; at the same time, the number of blebbed hepatocytes excluding trypan blue-stained hepatocytes was also counted and was expressed as the percentage of viable hepatocytes exhibiting multiple surface protrusions (cell blebs). The initial cell viability in each experiment was more than 85 %.

Synthesis of 2,4-dinitrophenyl *S*-conjugate of NAC (DNP-NAC) and determination of its conjugate

The 2,4-dinitrophenyl *S*-conjugate of NAC was prepared as described by Hinchman et al. (1991), using 1-fluoro-2,4-dinitrobenzene as a derivatizing agent and was identified by LC–MS and ^{1}H-NMR. ^{1}H-NMR spectra were obtained with a model JNM-A500 spectrometer (JOEL Ltd, Tokyo, Japan) operated at 500 MHz. Tetradeuteromethanol (methanol-d_4) was used as a solvent, and all chemical shifts (ppm) were referenced to the intrinsic value for the solvent. The chemical shifts and assignments for ^{1}H were as follows: δ 1.98 (s, 3H), 3.43–3.76 (m, 2H), 4.72–4.75 (m, 1H), 7.92–8.07 (d, 1H), 8.45–8.47 (d, 1H), and 8.96–8.97 (d, 1H). The negative electrospray ionization (−ESI)/MS spectrum of DNP-NAC conjugate showed a peak at m/z 328, corresponding to $[M–H]^-$. After NAC in hepatocyte suspensions was reacted with 1-fluoro-2,4-dinitrobenzene, chemical shifts of its derivative obtained were corresponded to the data showed by Hinchman et al. (1991) and Pombrio et al. (2001).

Determination of mitochondrial membrane potential

Mitochondrial membrane potential (MMP) in hepatocytes was determined with rhodamine 123, a fluorescence probe which selectively enters mitochondria with an intact membrane potential and is retained in the mitochondria (Lemasters et al. 1993). Hepatocytes (1×10^6 cells/ml) were preincubated with NAC dissolved in Krebs–Henseleit buffer (final concentrations 1, 2.5, and 5 mM) for 20 min before